Research Article

ATM kinase phosphorylates Ser15 of p53 in a pH-dependent manner

Serap Pektaş

Recep Tayyip Erdogan University, Faculty of Arts and Sciences, Department of Chemistry, 53020, Rize, TÜRKİYE
e-mail: serap.pektas@erdogan.edu.tr, ORCID: 0000-0003-0497-6257

Edited by:
Özkan Danış

Key words:
ATM kinase
Enzyme-substrate interactions
Kinase assays
p53

Abstract: The phosphorylation of Ser15 in the transactivation domain (TAD) of the tumor suppressor protein 53 (p53) by ataxia-telangiectasia mutated (ATM) kinase is a crucial step in the tumor suppressor function of p53. An understanding of the factors that affect the rate of Ser15 phosphorylation may provide new strategies for the manipulation of the ATM-p53 pathway in cancer therapy. In this study, the effect of electrostatic interactions between ATM and p53 was investigated by measuring the phosphorylation of Ser15 at varying pH ranges from 5 to 9. To achieve this, two different kinase assay methods were utilized: the ELISA technique, which directly quantifies the phosphorylated Ser15, and the Universal Kinase Assay, which assesses the formation of ADP. The results revealed that Ser15 phosphorylation was pH-dependent, with higher phosphorylation rates observed in the alkaline range. To ascertain whether the lower phosphorylation rates observed at acidic pH were due to protein denaturation, a pH-dependent solubility profile was generated using the CamSol server. The obtained results demonstrated comparable solubility rates within the pH range of the kinase assays performed. Furthermore, the significance of negatively charged residues in TAD$_{1-39}$ was evaluated by substituting Asp and Glu residues with hydrophobic and uncharged hydrophilic residues in TAD$_{1-39}$ using ChimeraX and subsequently comparing their interactions with the ATM using the protein-protein docking server HADDOCK2.4. The results of the docking simulations indicated that the alteration of negatively charged residues with uncharged ones resulted in a reduction in the efficiency of the interaction between the ATM and TAD$_{1-39}$. In conclusion, it can be stated that electrostatic interactions between the ATM and TAD are important for optimal Ser15 phosphorylation.

Özet: Tümör baskılayıcı protein 53'ün (p53) transaktivasyon domainindeki (TAD) Ser15'in ataksi-telenjiektazi mutasyonlu (ATM) kinaz tarafından fosforilasyonu, p53'ün tümör baskılayıcı işlevinde çok önemli bir adımdır. Ser15 fosforilasyon oranını etkileyen faktörlerin anlaşılması, kanser tedavisinde ATM-p53 yolağının manipülasyonu için yeni stratejiler sağlayabilir. Bu çalışmada, ATM ve p53 arasındaki elektrostatik etkileşimlerin etkisi, Ser15'in 5 ila 9 arasında değişen pH aralıklarında fosforilasyonu ölçülerek araştırılmıştır. Bunu başarmak için iki farklı kinaz tahlil yöntemi kullanılmıştır: fosforile Ser15'i doğrudan ölçen ELISA tekniği ve ADP oluşumunu değerlendiren Universal Kinase Assay. Sonuçlar, Ser15 fosforilasyonunun pH'a bağlı olduğunu ve alkali aralıkta daha yüksek fosforilasyon oranlarının gözlendiğini ortaya koymuştur. Asidik pH'da gözlenen daha düşük fosforilasyon oranlarının protein denatürasyonundan kaynaklanıp kaynaklanmadığını tespit etmek için CamSol sunucusu kullanılarak pH'ya bağlı bir çözünürlük profili oluşturulmuştur. Elde edilen sonuçlar, gerçekleştirilen kinaz deneylerinin pH aralığı içinde karşılaştırılabilir çözünürlük oranları göstermiştir. Ayrıca, TAD$_{1-39}$'daki negatif yüklü kalıntıların önemi, ChimeraX kullanılarak TAD$_{1-39}$'daki Asp ve Glu kalıntılarının hidrofobik ve yüksüz hidrofilik kalıntılarla değiştirilmesi ve ardından protein-protein yerleştirme sunucusu HADDOCK2.4 kullanılarak ATM ile etkileşimlerinin karşılaştırılmasıyla değerlendirilmiştir. Yerleştirme simülasyonlarının sonuçları, negatif yüklü kalıntıların yüksüz olanlarla değiştirilmesinin ATM ve TAD$_{1-39}$ arasındaki etkileşimin etkinliğinde bir azalmaya yol açtığını göstermiştir. Sonuç olarak, ATM ve TAD arasındaki elektrostatik etkileşimlerin optimal Ser15 fosforilasyonu için önemli olduğu söylenebilir.

Introduction

Ataxia-telangiectasia mutated (ATM) kinase is a member of the phosphatidylinositol 3-kinase-related kinases (PIKKs) family. The ATM protein, which is approximately 346 kDa in size, is encoded by the *ATM*

gene, and is located on chromosome 11q22-23 (Banin *et al.* 1998 Canman & Lim 1998, Li *et al.* 2020). ATM kinase phosphorylates its substrates at a serine or threonine residue preceding a glutamine residue (SQ/TQ motif) (Traven & Heierhorst 2005). The kinase domain (KD) of ATM is located in the C-terminal region and exhibits a high degree of homology to the phosphatidylinositol 3-kinases (PI3Ks) family of lipid kinases. ATM kinase has been shown to phosphorylate over one hundred substrates involved in DNA damage repair, cell cycle checkpoints, and apoptosis (Kastan & Lim 2000). The tumor suppressor protein 53 (p53) is one of the well-known substrates of ATM. In the absence of DNA double-strand breaks (DSBs), p53 is continuously expressed and degraded in cells (Ozaki & Nakagawara 2011). However, upon the occurrence of DSBs, the ATM kinase is activated and phosphorylates the p53 protein at the Ser15 residue within the transactivation domain (TAD) (Dumaz & Meek 1999). The p53 protein is encoded by the *TP53* gene, which is one of the most frequently mutated genes in human cancers (Goh *et al.* 2011, Bouaoun *et al.* 2016, Marei *et al.* 2021). The Ser15 phosphorylation event stabilizes p53 and facilitates its transactivation function. Stabilized p53 transactivates genes involved in apoptosis, cell cycle arrest, DNA repair, and other processes. Given the role of ATM and p53 in cancer biology, elucidating the factors that regulate the Ser15 phosphorylation event is of significant importance for controlling its function and may ultimately contribute to the cancer therapy targeting ATM and p53-dependent pathways (Yogosawa & Yoshida 2018, Cheng *et al.* 2018, Marei *et al.* 2021). The factors influencing enzyme-substrate recognition and substrate specificity include electrostatic interactions, hydrogen bonding, hydrophobic interactions, and Van der Waals forces. By modifying or blocking these interactions through a molecule, residue modification, or by changing the charge of interacting residues, it is possible to manipulate enzymatic activity (Hansen *et al.* 2005, Fadeyi *et al.* 2017, Lin 2023.

Amino acid residues with ionizable side chains such as Asp, Glu, His, Lys, and Arg can play a crucial role in enzyme-substrate recognition. These residues facilitate electrostatic interactions, which may influence the specificity of protein interactions. Modulating the charges of these residues by pH or post-translational modifications could disrupt protein-protein interactions (Schreiber *et al.* 2009, Zhou & Pang 2018). The three-dimensional (3D) structure of the ATM kinase domain, resolved by cryo-electron microscopy, reveals an active site opening lined predominantly with positively charged and hydrophobic residues. In contrast, the TAD sequence of p53 contains 16 negatively charged residues (Table 1). Given that electrostatic interactions can occur even at relatively large distances (5-10 Å) and are critical for the specificity of protein-protein recognition (Schreiber *et al.* 2009), the charge distribution in the active site region of ATM and the TAD of p53 suggests that electrostatic interactions may play a role in ATM-TAD recognition (Fig. 1). Previous mutational studies have demonstrated that prolines and hydrophobic residues within the TAD are essential for its transactivation function and interaction with its negative regulator mouse double minute 2 homolog (MDM2), as well as the Taz1 and Taz2 domains of coactivator p300 (Grossman 2001, Feng *et al.* 2009, Teufel *et al.* 2009, Miller *et al.* 2015, Li *et al.* 2022). Furthermore, the double TAD^{E2E3} or TAD^{D41D42} mutations have also been reported to affect the transactivation function of p53, although to a lesser extent than prolines and hydrophobic residues (Chang *et al.* 1995). However, the contribution of these residues to the Ser15 phosphorylation event remains to be elucidated.

In this study, to determine the effect of electrostatic interactions on the ATM-TAD interaction, the phosphorylation of Ser15 of p53 was monitored at a varying pH range from 5 to 9. In addition to kinase assays to elucidate the contribution of electrostatic interactions, two TAD variants were generated by replacing the negatively charged residues in TAD_{1-39} with either Asn and Gln or with Leu, and their interactions with the ATM kinase, were evaluated through protein-protein docking using HADDOCK2.4 (Van Zundert *et al.* 2016).
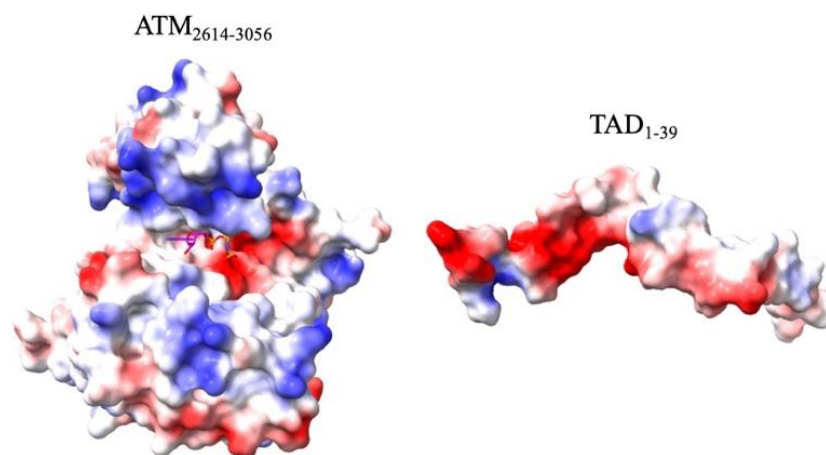
Fig. 1. Surface charge of $ATM-KD_{2614-3056}$ and TAD_{1-39}. Red colors represent negative charge, white regions are neutral, and blue regions are positively charged (Image generated by UCSF ChimeraX) (Meng *et al.* 2023).

Materials and Methods

All chemicals were purchased from commercial vendors and used as received, except for the human p53 and human ATM expression plasmids. Recombinant human p53 plasmid (corresponding to residues 1-393) was a gift from Cheryl Arrowsmith (Addgene plasmids # 24859; https://www.addgene.org/24859/; RRID: Addgene_24859) (Ayed *et al*. 2001). Recombinant human full-length ATM plasmid pcDNA3.1(+)Flag-His-ATM wt was a gift from Michael Kastan (Addgene plasmid # 31985; https://www.addgene.org/31985/; RRID:Addgene_31985) (Canman *et al*. 1998). *E. coli* BL21(DE3)plysS cells and 10 kDa dialysis tubing were purchased from Thermo Fisher Scientific. QIAprep Spin Miniprep Kit (#27106, QIAGEN) and PureLink HiPure Plasmid Maxiprep Kit (#K210007, Invitrogen) were used for plasmid DNA isolation. LB broth miller, ATP, $MgCl_2$, $MnCl_2$, ampicillin, chloramphenicol, Ni-NTA affinity resin, and imidazole were purchased from Merck. Isopropyl β-D-1-thiogalactopyranoside (IPTG) purchased from Biogen. Universal Kinase Assay Kit (Fluorometric) (ab138879) and Human p53 ELISA Kit (pSer15) were purchased from Abcam (ab156027).

p53 Transformation and Expression

DH5α cells containing recombinant human p53 plasmid were grown overnight at 37°C in a shaker incubator. Plasmid DNA was then isolated using the QIAprep Spin Miniprep Kit (QIAGEN, USA) according to the kit instructions. The isolated plasmid was transformed into the *E. coli* BL21(DE3)pLysS cells by the heat shock method (Froger & Hall 2007). In summary, the *E. coli* BL21(DE3)pLysS competent cells were incubated with the isolated plasmid at 42°C for 45 seconds, and then placed on ice. Subsequently, 500 μL of SOC media was added to the cell-plasmid mixture, which was then incubated at 37°C for 1 hour. The plasmid-transformed cells were identified based on their capacity to form bacterial colonies on an ampicillin-containing plate. Subsequently, p53 was expressed as previously described with some modifications. Briefly, *E. coli* BL21(DE3)plysS cells transformed with the human p53 gene were grown overnight in a 220-rpm shaking incubator at 37°C in 25 mL of LB broth (Miller) medium containing 100 μg/mL ampicillin and 37 μg/mL chloramphenicol. The next morning, 4 mL of the overnight culture was inoculated into 400 mL of LB broth (Miller) medium containing ampicillin and chloramphenicol. When the OD_{600nm} reached 0.5-0.6, IPTG was added to a final concentration of 1 mM to induce the cells. After IPTG induction, the cells were incubated at 20°C for 6 hours. Finally, the cells were harvested by centrifugation at 8,000 rpm and stored at -86°C for later purification.

p53 Purification

Recombinant human p53 was purified as previously described with some modifications (Ayed *et al*. 2001). Cells were lysed in a lysis buffer (50 mM NaH_2PO_4, pH 8.00, 0.3 M NaCl, 10 mM imidazole, 1% glycerol, 0.1% tween, 1 mM DTT, 0.5 mM PMSF) and sonication was used to lyse the cells (5 seconds on, 10 seconds off, and 30% amplitude for 3-5 minutes). After sonication, the pellet was removed by centrifugation (at 15,000 rpm for 40 minutes). The obtained supernatant was applied to the Ni-NTA column at a flow rate of 0.25 min/mL. The column was then washed with the five-column volume of wash buffer (lysis buffer minus DTT, plus 25 mM imidazole, 5 mM ATP, 1 mM $MgCl_2$, and 1 M NaCl). The purified protein was eluted with a buffer containing 250 mM imidazole. The eluted protein was then buffer exchanged to 50 mM Tris-HCl pH 8.00 by dialysis and stored at -20°C. The purity of the protein was confirmed by polyacrylamide gel electrophoresis (SDS-PAGE) (Shapiro *et al*. 1967) (Fig. 3a).

Transient Transfection of ATM in Expi293F Cells

Stbl2 cells containing the recombinant human ATM plasmid were grown in a shaker incubator for 24 hours at 30°C. Plasmid DNA was then isolated using a PureLink HiPure Plasmid Maxiprep Kit (Thermo Fisher Scientific, USA). Expi293F cells were grown in an Expi293 expression medium to a cell density of 2×10^6 cells/mL. PEI 40K Max was used as the transfection reagent (Baretić *et al*. 2017). PEI was dissolved in Expi293 expression medium and then added dropwise to the isolated DNA in a final ratio of 1:3 (PEI: DNA). After 15 min of incubation at room temperature, the PEI-DNA mixture was added dropwise to Expi293F cells. 24 hours after transfection, a fresh Expi293F expression medium was added to the transfected cells. At 72 hours post-transfection, the cells were harvested at 4,500 rpm and stored at -86°C for later purification.

ATM Purification

Recombinant human ATM was purified as described previously (Baretić *et al*. 2017). Briefly, Expi293F cells transiently transfected with human ATM plasmid were lysed in lysis buffer (50 mM Tris-HCl, pH 8.00, 0.3 M NaCl, 1.0 mM DTT, 0.5 mM PMSF, 10% glycerol). The cells were then homogenized with 50 strokes using a Dounce homogenizer. The homogenate was centrifuged at 14,500 rpm for 45 min at 4°C. The resulting cell lysate was mixed with anti-Flag M2 affinity gel and incubated for 1 hour at 4°C on a benchtop rotator. The cell lysate gel mixture was then loaded onto an empty chromatography column. The column was washed with five times the column volume of lysis buffer. Finally, ATM was eluted from the column using Flag peptide (2 μg/mL). The purity of the eluted protein was checked using SDS-PAGE (Shapiro *et al*. 1967) (Fig. 3b). Flag peptide was removed by dialysis using 10k snakeskin dialysis tubing in 50 mM Tris-HCl pH 8.00, 10% glycerol.

Kinase Activity Assays

A fluorometric-based universal kinase assay measuring ADP formation and ELISA measuring phosphorylated Ser15 were applied to monitor kinase activity. All activity assays were performed with saturating concentrations of ATP (800 μM), $MgCl_2$ (20 mM), $MnCl_2.H_2O$ (20 mM), ATM (25 nM), and p53 (25

μM). To study the effect of pH on Ser15 phosphorylation, a buffer cocktail containing 25 mM MES and 25 mM Tris-HCl was prepared to obtain acidic, neutral, and basic pH ranges. ATM and p53 were added to the buffer cocktails, and each kinase reaction was initiated by adding the ATP-Mg^{2+}-Mn^{2+} complex to the reaction mixture. The reactions were then quenched by the addition of a stop solution (12.5 mM HEPES, pH 8.00, 1% glycerol, 250 mM EDTA) after 15 minutes. For each reaction, phosphorylated Ser15 ($Ser15^P$) was measured using a p53 (pS15) ELISA kit, and ADP formation was determined using a fluorometric-based Universal Kinase Assay Kit according to the kit instructions (Abcam, #ab138879).

Stability Prediction of ATM and p53 at Different pH Values

The stabilities of ATM kinase and p53 were predicted at different pH ranges using the CamSol server (Sormanni *et al*. 2015). For this purpose, the amino acid sequences of human ATM_{1-3056} and human $p53_{1-393}$ were obtained from the NCBI website (the accession number for ATM kinase is AAB65827.1, and for p53 it is BAC16799.1) (Sayers *et al*. 2022). The pH range was set from 1 to 14 for the predictions. Since proteins are unstable at their isoelectric point (p*I*), in addition to stability at different pH values, the p*I* of ATM_{1-3056} and $p53_{1-393}$ was determined based on their amino acid sequences using the ExPASy ProtParam tool (Wilkins *et al*. 1999) and avoided in kinase assays (p*I* of ATM is 6.39 and of p53 is 6.33).

ATM and TAD_{1-39} Docking

In docking experiments, the 3D structures of TAD and ATM, which are available in the Protein Data Bank (PDB), were used. For the TAD, the 3D structure with PDB ID: 2k8f, which contains the TAD_{1-39} chain, was utilized as a template, and the remaining chains were removed (Feng *et al*. 2009). For the $ATM-KD_{2614-3056}$ structure, the PDB structure with the PDB ID 8oxo was used as a template (Howes *et al*. 2023). The effect of negatively charged residues on the ATM-TAD interaction was investigated by generating two variants, using ChimeraX (Meng *et al*. 2023). One variant was generated by changing two Asp residues to Asn and five Glu residues to Gln in TAD_{1-39} (TAD^{NQ}), maintaining similar steric effects while eliminating the charge effect. The other variant was generated by replacing Asp and Glu residues with Leu, thus eliminating polar character (TAD^L). The HADDOCK2.4 server was utilized for $ATM-TAD_{1-39}$ docking predictions (Van Zundert *et al*. 2016, Honorato *et al*. 2021). The docking employed to the C-terminal region of $ATM_{2614-3056}$, with the remaining residues in the 8oxo PBD structure removed. Actively interacting residues were defined based on the $ATM_{1462-3056}-TAD_{12-18}$ structure complex (PDB ID: 8oxo) (Fig. 2). In the TAD_{1-39} structure, the residues Leu14, Ser15, and Gln16 were identified as actively interacting. Similarly, in the $ATM_{2614-3056}$ structure, residues His2872, Thr2902, and Phe3049 were identified as actively interacting (Fig. 2). The docking was performed for the TAD^{WT}, TAD^{NQ} and TAD^L variants (Table 1).
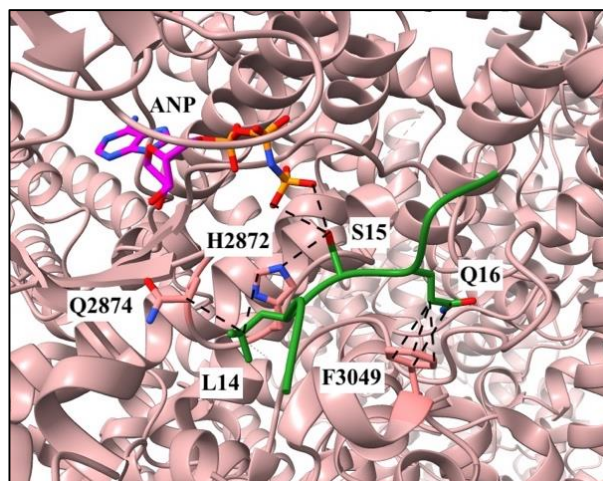
Fig. 2. The active site of the ATM interacting with TAD_{12-18} (shown in green) (PDB ID: 8oxo), ANP is a structural analogue of ATP (image generated by UCSF ChimeraX) (Meng *et al*. 2023).

Table 1. The amino acid sequences of the wild-type TAD_{1-39} (TAD^{WT}) and its TAD^{NQ} and TAD^L mutant variants.

| TAD_{1-39}	Sequence
TAD^{WT}	MEEPQSDPSVEPPLSQETFSDLWKLLPENNVLSPLPSQA
TAD^{NQ}	MQQPQSNPSVQPPLSQQTFSNLWKLLPQNNVLSPLPSQA
TAD^L	MLLPQSLPSVLPPLSQLTFSLLWKLLPLNNVLSPLPSQA

Results

Effect of pH on Ser15 Phosphorylation

Kinase assays were conducted using a saturating concentration of ATP, Mg^{2+}, and $p53_{1-393}$ to ensure maximal kinase activity in pH-adjusted buffers. The formation of precipitates in kinase reactions was observed at the physiological temperature of 37°C. To prevent protein denaturation, kinase assays were performed at room temperature (approximately 20°C). The pH dependency of Ser15 phosphorylation was observed over the pH range of 5 to 9. Phosphorylation occurred at a faster rate at the basic pH values than at the acidic pH values (Figs 4a, b). The phosphorylation rate was found to be lowest at pH 5, with an increase observed as the pH increased, reaching a maximum in the pH range of 7 to 9. Due to the tendency of the ATM denaturation to occur at pH values below 5 and above 9, these pH values were avoided. Both methods gave comparable pH profiles.

The pH Stability Profile of ATM and p53

The full-length ATM_{1-3056} exhibits a negative solubility score between pH 1 and 14 (-3.80639 to -3.07764), indicating poor solubility (Fig. 5a). However, within the pH range of the kinase assay (pH 5 to 9), the solubility scores are relatively close, -3.71628 to -3.79001, differing by only about 0.07373 unit of solubility. In comparison to ATM, p53 showed generally higher solubility scores, ranging from 1.78721 to 2.0416, over the pH range of 1 to 14 (Fig. 5b).
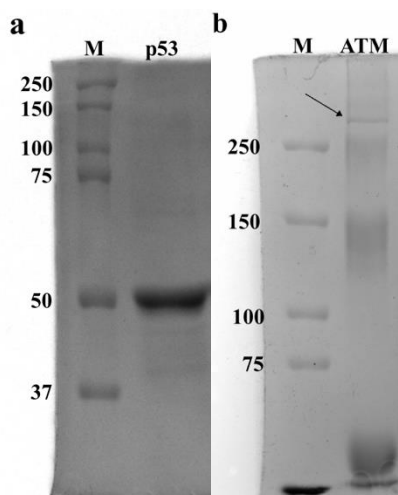
Fig. 3. The SDS-PAGE and Coomassie blue staining of the purified p53 and ATM. **a.** Purified p53 was loaded onto 5% stacking gel and 10% separating gel, M: protein marker (10-250 kDa), **b.** purified ATM was loaded onto 4% stacking gel and 6% separating gel. The arrow points to the ATM band at around 346 kDa, M: protein marker (10-250 kDa).
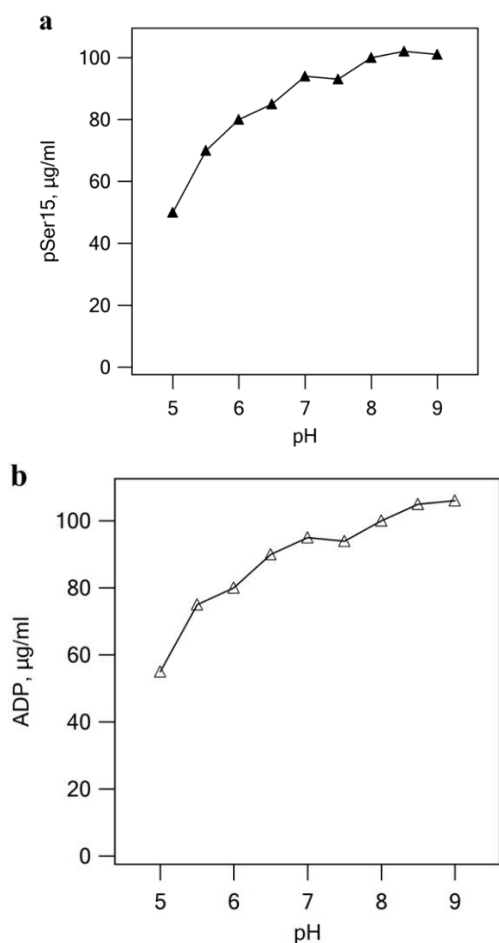
Fig. 4. The pH profile of Ser15 phosphorylation. **a.** pH profile using the Human p53 (pSer15) ELISA Kit, **b.** pH profile using the ADP-based Universal Kinase Assay Kit (Fluorometric).
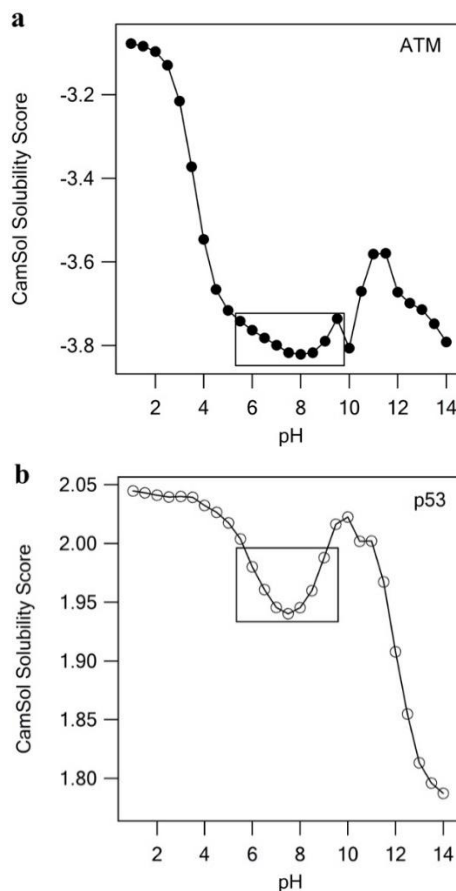
Fig. 5. pH solubility profile generated by the CamSol server (Sormanni *et al*. 2015). **a.** ATM_{1-3056}, pH solubility profile, **b.** $p53_{1-393}$, pH solubility profile. The pH range of the kinase assay is indicated by a rectangle.

In the kinase assay pH range (5 to 9), the solubility scores of p53 exhibited a range of 2.01747 to 1.98791, with a difference of 0.02956 units. Overall, p53 appears to be more stable than ATM.

### *The Importance of Charged Residues of TAD$_{1-39}$ on ATM-TAD Recognition*

To evaluate the importance of the negatively charged residues in TAD_{1-39}, two mutant TAD_{1-39} variants were generated by replacing two Asp residues with Asn or Leu and five Glu residues with Gln or Leu within the TAD_{1-39} using ChimeraX (Meng *et al.* 2023). The interaction of these variants with the kinase domain of ATM was then analyzed using the HADDOCK2.4 server (Honorato *et al.* 2021; Van Zundert *et al.* 2016). The generated docking complexes were evaluated based on their HADDOCK2.4 scores, with more negative scores indicating stronger interactions. The most reliable docking complex in HADDOCK2.4 is identified based on the more negative z-scored complexes among the generated structures. The interaction energies of both the TAD^{WT}, TAD^{NQ}, and TAD^{L} domains with the $ATM_{2614-3056}$ are presented in Table 2. The HADDOCK2.4 scores indicate that the ATM-TAD^{WT} complex exhibits a higher interaction

efficiency compared to the ATM-TAD^{NQ} and ATM-TAD^{L} variants (Table 2). Conversely, the ATM-TAD^{NQ} and ATM-TAD^{L} complexes showed relatively similar and lower interaction efficiencies than the ATM-TAD^{WT} complex. Significant reductions were observed in the electrostatic energies, which decreased from -341.6 to -192.7 for the ATM-TAD^{NQ} complex and to -221.8 for the ATM-TAD^{L} complex in comparison to the ATM-TAD^{WT} complex. Another notable difference was observed in the desolvation energies. The ATM-TAD^{WT} complex had a desolvation energy of -8.2, which increased to -28.2 for the ATM-TAD^{NQ} complex and to -24.8 for the ATM-TAD^{L} complex. The hydrophobic interactions were found to be comparable between TAD^{WT}, TAD^{NQ}, and TAD^{L}, with -36.3, -33.5, and -34.4, respectively. Overall, replacement of acidic residues on TAD$_{1-39}$ with uncharged or hydrophobic residues resulted in alterations to the residues involved in the ATM-TAD interaction. The list of residues involved in this interaction is provided in Table 3.

The structural alignment of the ATM-TAD$_{1-39}$ complexes demonstrates the change in binding orientation (Figs 6a-d). In the ATM-TAD^{WT} complex, TAD$_{1-39}$ exhibited a predominant interaction with residues between 2 and 21, whereas TAD^{NQ} demonstrated a more pronounced interaction with residues between 9 and 24, with Gln5 also involved in the interaction. In contrast, the TAD^{L} variant, which has fewer residues supporting electrostatic interactions, exhibited a predominant interaction with residues between 15 and 31. A more detailed examination of the ATM-TAD complexes, focusing on the residues involved in the interaction within a 3.5 Å distance, is presented in Figs 6e to 6f. The Phe19 of TAD$_{1-39}$ has a conserved interaction with ATM residues (Pro2901, Thr2902, Phe3049) in both TAD^{WT} and its mutant variants (Figs 6e-f). In addition to Phe19 residue, Leu14, Ser15, Gln16, and Glu17 residues of TAD$_{1-39}$ are also involved in the interaction with ATM, albeit with different residue contacts. Furthermore, Gln2802, Asp2870, and Lys3053 within ATM are also involved in stabilizing the ATM-TAD$_{1-39}$ interaction.

Table 2. HADDOCK2.4 docking energy scores for ATM-TAD^{WT}, ATM-TAD^{NQ}, and ATM-TAD^{L} complexes.

TAD$_{1-39}$	HADDOCK Score	Electrostatic energy	Van der Waals energy	Desolvation energy	Z-Score
TAD^{WT}	-111.7 ± 7.1	-341.6 ± 51.0	-36.3 ± 2.9	-8.2 ± 2.6	-1.6
TAD^{NQ}	-99.5 ± 5.7	-192.7 ± 19.4	-33.5 ± 3.1	-28.2 ± 1.2	-1.3
TAD^{L}	-100.3 ± 12.5	-221.8 ± 34.5	-34.4 ± 1.9	-24.8 ± 1.5	-2.0
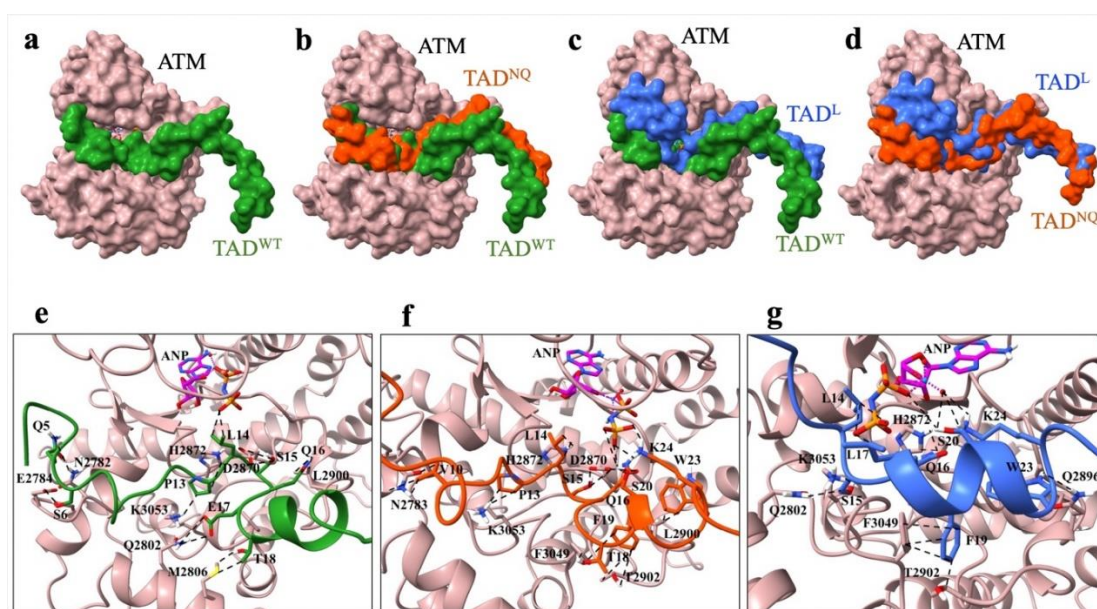
Fig. 6. ATM$_{2614-3056}$-TAD$_{1-39}$ interactions. **a.** ATM$_{2614-3056}$-TAD^{WT} complex surface representation, **b.** ATM$_{2614-3056}$-TAD^{WT} and ATM$_{2614-3056}$-TAD^{NQ} complexes alignment. **c.** ATM$_{2614-3056}$-TAD^{WT} and ATM$_{2614-3056}$-TAD^{L} complexes alignment surface depictions, **d.** ATM$_{2614-3056}$-TAD^{NQ} and ATM$_{2614-3056}$-TAD^{L} complexes alignment surface depictions, **e.** ATM$_{2614-3056}$-TAD^{WT} complex interacting residues around the active site, **f.** ATM$_{2614-3056}$-TAD^{NQ} complex interacting residues around the active site, **g.** ATM$_{2614-3056}$-TAD^{L} complex interacting residues around the active site (ANP is a structural analogue of ATP) (Images were generated by UCSF ChimeraX) (Meng *et al.* 2023).

Table 3. Residues involved in the ATM$_{2614-3056}$-TAD$_{1-39}$ interaction within up to 4 Å of each other.

TAD^{WT}/TAD^{NQ}/ TAD^{L}	ATM-(TAD^{WT})	ATM-(TAD^{NQ})	ATM-(TAD^{L})
E2/Q2/L2	R2642, Q2641, K2643	-	-
E3/Q3/L3	R2691, K2643	-	-
P4	R2642	-	T2640
Q5	N2782, E2783	E2784	-
S6	N2783, E2784	-	-
D7/N7/L7	R2642	-	K2636
P8	-	-	-
S9	N2783	F2799	-
V10	N2783	N2783	-
E11/Q11/L11	K3053	K3053	ANP
P12	-	-	ANP
P13	K3053	K3053	-
L14	H2872, ANP	H2872	ANP
S15	D2870, H2872	D2870, H2872	Q2802, K3053
Q16	L2900, P2901	D2870	D2870, H2872, F3049
E17/Q17/L17	Q2802, M2806	Q2802	ANP
T18	M2806	F3049	-
F19	P2901, T2902, F3049	P2901, T2902, F3049	P2901, T2902, F3049
S20	-	V2696, ANP	ANP
D21/N21/L21	V2696	-	-
L22	-	P2901	P2901
W23	-	L2900	V2891, Q2896
K24	-	V2696, ANP	ANP
L28	-	-	N2963
N29	-	-	T2961, M2962
V31	-	-	N2963

Discussion

The Ser15 phosphorylation of the highly dynamic and acidic TAD of p53 is known to be important for its transactivation function and cellular stability (Kubbutat *et al.* 1997, Dumaz & Meek 1999, Jenkins *et al.* 2012). However, the factors that are affecting this phosphorylation event need further investigation. The present results indicate that electrostatic interactions between ATM and TAD play a role in efficient phosphorylation of Ser15. Modulation of charged amino acid side chains by pH led to a change in the Ser15 phosphorylation rate. The higher phosphorylation rates were observed at basic pH ranges compared to acidic pH ranges (Figs 3a, b). This alteration in the phosphorylation rate with pH indicates that electrostatic interactions between relatively positively charged residues in the active site opening of ATM and negatively charged residues in TAD may be significant for optimal ATM-TAD recognition (Fig. 1). The results also suggest that electrostatic interactions may be used to regulate Ser15 phosphorylation, a process that is of critical importance in the ATM and p53-mediated pathway in cancer biology.

The modulation of ionizable amino acid side chains by pH may affect protein structural stability through alterations to side-chain interactions that form folded protein, potentially may lead to denaturation (Schaefer *et al.* 1997, Tollinger *et al.* 2003). The structural stability of ATM$_{1-3056}$ and p53$_{1-393}$ at varying pH ranges was evaluated using the CamSol server (Sormanni *et al.* 2015). According to the CamSol sever result, similar solubility scores in the kinase assay pH range suggest a low likelihood of pH-dependent denaturation (Fig. 5b). The pH-dependent solubility profiles of ATM$_{1-3056}$ and p53$_{1-393}$ provide evidence that changes in electrostatic interactions, rather than denaturation, may be responsible for the observed decrease in phosphorylation rate. Nevertheless, this prediction requires experimental validation to substantiate the conclusions drawn.

A reduction in electrostatic interactions is observed for both TAD^{NQ} and TAD^{L} variants in comparison to TAD^{WT}, indicating that the negatively charged residues in TAD^{WT} play a crucial role in stabilizing the interaction through electrostatic forces. In the mutants, the remaining polar residues (6, Ser; 3, Gln; 2, Asn; 1, Thr) can provide hydrogen bonding and other polar interactions, but they are unable to fully compensate for the loss of the strong electrostatic interactions provided by the acidic residues, thereby compromising binding efficiency. In addition to the observed changes in electrostatic interactions, alterations in desolvation energies were also observed in the TAD^{NQ} and TAD^{L} variants. The TAD^{NQ} and TAD^{L} variants exhibited a considerable increase in desolvation energy compared to the TAD^{WT}. These indicate that the replaced residues in TAD^{NQ} and TAD^{L} are less favorable for interaction in an aqueous environment, potentially due to their uncharged and hydrophobic nature. In contrast to the electrostatic and desolvation energies, the hydrophobic interactions were relatively similar across all variants, suggesting that replacing the charged residues with uncharged or hydrophobic ones does not significantly affect the hydrophobic components of the interaction (Table 2). In addition to the alteration of interaction energies, the orientation of the ATM-TAD interface also changed for TAD^{NQ} and TAD^{L} compared to

TAD^{WT}. In the TAD^{WT}, the interaction was predominantly observed in the more polar N-terminal region. In contrast, in TAD^{NQ}, the interaction shifted to the central region due to the loss of electrostatic characteristics at the N-terminal region. In the TAD^L variant, the interaction interface shifted to the C-terminal region, which contains a greater proportion of polar amino acids than the N-terminal region. These results further illustrate the significance of the electrostatic interactions in the ATM-TAD interaction. These findings contribute to a more comprehensive understanding of the molecular mechanisms underlying ATM-TAD recognition.

Conclusion

The results of this study highlight the critical role of electrostatic interactions between the kinase domain of ATM and the TAD of p53 in facilitating Ser15 phosphorylation. The observed variations in phosphorylation rate across different pH ranges indicate that these electrostatic interactions play an important role in regulating the optimal interaction between ATM and TAD. Moreover, the CamSol solubility predictions support the notion that the observed changes in phosphorylation rate are not primarily due to pH-dependent stability issues. Furthermore, exploration of negatively charged residues within the TAD by residue substitution and subsequent protein-protein docking

revealed that these residues are indeed essential for optimal interaction between ATM and TAD. Taken together, these results demonstrate the importance of electrostatic interactions between ATM and TAD for optimal Ser15 phosphorylation and further our understanding of the molecular mechanisms underlying ATM-p53 signaling.

References

1. Ayed, A., Mulder, F.A., Yi, G.S., Lu, Y., Kay, L.E. & Arrowsmith, C.H. 2001. Latent and active p53 are identical in conformation. *Nature structural biology*, 8(9): 756-760. https://doi.org/10.1038/nsb0901-756

2. Banin, S., Moyal, L., Shieh, L., Taya, Y., Anderson, C.W., Chessa, L., Prives, C., Reiss, Y., Shiloh, Y. & Ziv, Y. 1998. Enhanced Phosphorylation of P53 by ATM in Response to DNA Damage. *Science*, 281(5383): 1674-77. https://doi.org/10.1126/science.281.5383.1674

3. Baretić, D., Pollard, H.K., Fisher, D.I., Johnson, C.M., Santhanam, B., Truman, C.M. & Williams, R.L. 2017. Structures of closed and open conformations of dimeric human ATM. *Science advances*, 3(5): e1700933. https://doi.org/10.1126/sciadv.1700933

4. Bouaoun, L., Sonkin, D., Ardin, M., Hollstein, M., Byrnes, G., Zavadil, J. & Olivier, M. 2016. TP53 variations in human cancers: new lessons from the IARC TP53 database and genomics data. *Human mutation*, 37(9): 865-876. https://doi.org/10.1002/humu.23035

5. Canman, C.E., Lim, D.S., Cimprich, K.A., Taya, Y., Tamai, K., Sakaguchi, K., Appella, E., Kastan, M.B. & Siliciano, J.D. 1998. Activation of the ATM Kinase by Ionizing Radiation and Phosphorylation of P53. *Science,* 281(5383): 1677-79. https://doi.org/10.1126/science.281.5383.1677

6. Canman, C.E. & Lim, D.S. 1998. The role of ATM in DNA damage responses and cancer. *Oncogene*, 17(25), 3301-3308. https://doi.org/10.1038/sj.onc.1202577

7. Chang, J., Kim, D.H., Lee, S.W., Choi K.Y. & Sung, Y.C. 1995. Transactivation Ability of P53 Transcriptional Activation Domain Is Directly Related to the Binding Affinity to TATA-Binding Protein. *Journal of Biological Chemistry,* 270(42): 25014-25019. https://doi.org/10.1074/jbc.270.42.25014

8. Cheng, J., Dwyer, M., Okolotowicz, K.J., Mercola, M. & Cashman, J.R. 2018. A novel inhibitor targets both Wnt signaling and ATM/p53 in colorectal cancer. *Cancer Research*, 78(17): 5072-5083. https://doi.org/10.1158/0008-5472.CAN-17-2642

9. Dumaz, N. & Meek, D.W. (1999). Serine 15 phosphorylation stimulates p53 transactivation but does not directly influence interaction with HDM2. *The EMBO journal*, 18(24): 7002-7010. https://doi.org/10.1093/emboj/18.24.7002

10. Fadeyi, O.O., Hoth, L.R., Choi, C., Feng, X., Gopalsamy, A., Hett, E.C. & Jones, L.H. 2017. Covalent enzyme inhibition through fluorosulfate modification of a noncatalytic serine residue. *ACS Chemical Biology*, 12(8): 2015-2020. https://doi.org/10.1021/acschembio.7b00403

11. Feng, H., Lisa M. Miller Jenkins, L.M.M., Durell, S.R., Hayashi, R., Mazur, S.J., Cherry, S., Tropea, J.E., Miller, M., Wlodawer, A., Appella, E. & Bai., Y. 2009. Structural Basis for P300 Taz2-P53 TAD1 Binding and Modulation by Phosphorylation. *Structure,* 17(2): 202-210. https://doi.org/10.1016/j.str.2008.12.009

12. Froger, A. & Hall, J.E. 2007. Transformation of plasmid DNA into E. coli using the heat shock method. *JoVE*

(Journal of visualized experiments), (6): e253. https://doi.org/10.3791/253

13. Goh, A.M., Coffill, C.R. & Lane, D.P. 2011. The role of mutant p53 in human cancer. The Journal of pathology, 223(2): 116-126. https://doi.org/10.1002/path.2784

14. Grossman, S.R. 2001. p300/CBP/p53 interaction and regulation of the p53 response. *European journal of biochemistry*, 268(10): 2773-2778. https://doi.org/10.1046/j.1432-1327.2001.02226.x

15. Hansen, S.K., Cancilla, M.T., Shiau, T.P., Kung, J., Chen, T. & Erlanson, D.A. 2005. Allosteric inhibition of PTP1B activity by selective modification of a non-active site cysteine residue. *Biochemistry*, 44(21), 7704-7712. https://doi.org/10.1021/bi047417s

16. Honorato, R.V., Koukos, P.I., Jiménez-García, B., Tsaregorodtsev, A., Verlato, M., Giachetti, A., Rosato, A. & Bonvin, A.M. 2021. Structural biology in the clouds: the WeNMR-EOSC ecosystem. *Frontiers in molecular biosciences*, 8: 729513. https://doi.org/10.3389/fmolb.2021.729513

17. Howes, A.C., Perisic, O. & Williams, R.L. 2023. Structural insights into the activation of ataxia-telangiectasia mutated by oxidative stress. *Science Advances*, 9(39): eadi8291. https://doi.org/10.1126/sciadv.adi8291

18. Jenkins, L.M. M., Durell, S.R., Mazur, S.J. & Appella, E. 2012. p53 N-terminal phosphorylation: a defining layer of complex regulation. *Carcinogenesis*, 33(8): 1441-1449. https://doi.org/10.1093/carcin/bgs145

19. Kastan, M.B. & Lim, D.S. 2000. The many substrates and functions of ATM. *Nature reviews Molecular cell biology*, 1(3): 179-186. https://doi.org/10.1038/35043058

20. Kubbutat, M.H., Jones, S.N. & Vousden, K.H. 1997. Regulation of p53 stability by Mdm2. *Nature*, 387(6630): 299-303. https://doi.org/10.1038/387299a0

21. Li, T., Motta, S., Stevens, A.O., Song, S., Hendrix, E., Pandini, A. & He, Y. 2022. Recognizing the binding pattern and dissociation pathways of the p300 Taz2-p53 TAD2 complex. *JACS Au*, 2(8): 1935-1945. https://doi.org/10.1021/jacsau.2c00358

22. Li, W., Peng, X., Lang, J. & Xu, C. 2020. Targeting mouse double minute 2: current concepts in DNA damage repair and therapeutic approaches in cancer. *Frontiers in Pharmacology*, 11: 537486. https://doi.org/10.3389/fphar.2020.00631

23. Lin, H. 2023. Substrate-selective small-molecule modulators of enzymes: mechanisms and opportunities. *Current opinion in chemical biology*, 72: 102231. https://doi.org/10.1016/j.cbpa.2022.102231

24. Marei, H.E., Althani, A., Afifi, N., Hasan, A., Caceci, T., Pozzoli, G. & Cenciarelli, C. 2021. p53 signaling in cancer progression and therapy. *Cancer cell international*, 21(1): 703. https://doi.org/10.1186/s12935-021-02396-8

25. Meng, E C., Goddard, T.D., Pettersen, E.F., Couch, G.S., Pearson, Z.J., Morris, J.H. & Ferrin, T.E. 2023. UCSF ChimeraX: Tools for structure building and analysis. *Protein Science*, 32(11): e4792. https://doi.org/10.1002/pro.4792

26. Miller Jenkins, L.M., Feng, H., Durell, S.R., Tagad, H.D., Mazur, S.J., Tropea, J.E., Bai., T.Y. & Appella, E. 2015. Characterization of the p300 Taz2–p53 TAD2 complex and comparison with the p300 Taz2–p53 TAD1 complex. *Biochemistry*, 54(11): 2001-2010. https://doi.org/10.1021/acs.biochem.5b00044

27. Ozaki, T. & Nakagawara, A. 2011. Role of p53 in cell death and human cancers. *Cancers*, 3(1): 994-1013. https://doi.org/10.3390/cancers3010994

28. Sayers, E.W., Bolton, E.E., Brister, J.R., Canese, K., Chan, J., Comeau, D.C., Connor, R., Funk, K., Kelly, C., Kim, S., Madej, T., Marchler-Bauer, A., Lanczycki, C., Lathrop, S., Lu, Z., Thibaud-Nissen, F. & Sherry, S.T. 2022. Database resources of the national center for biotechnology information. *Nucleic acids research*, 50(D1): 20-26. https://doi.org/10.1093/nar/gkab1112

29. Schaefer, M., Sommer, M. & Karplus, M. 1997. pH-dependence of protein stability: absolute electrostatic free energy differences between conformations. *The Journal of Physical Chemistry B*, 101(9): 1663-1683. https://doi.org/10.1021/jp962972s

30. Schreiber, G., Haran, G. & Zhou, H.X. 2009. Fundamental aspects of protein− protein association kinetics. *Chemical reviews*, 109(3): 839-860. https://doi.org/10.1021/cr800373w

31. Shapiro, A.L., Viñuela, E. & Maizel Jr, J.V. 1967. Molecular weight estimation of polypeptide chains by electrophoresis in SDS-polyacrylamide gels. *Biochemical and biophysical research communications*, 28(5): 815-820. https://doi.org/10.1016/0006-291X(67)90391-9

32. Sormanni, P., Aprile, F.A. & Vendruscolo, M. 2015. The CamSol method of rational design of protein mutants with enhanced solubility. *Journal of molecular biology*, 427(2): 478-490. https://doi.org/10.1016/j.jmb.2014.09.026

33. Teufel, D.P., Bycroft, M. & Fersht, A.R. 2009. Regulation by phosphorylation of the relative affinities of the N-terminal transactivation domains of p53 for p300 domains and Mdm2. *Oncogene*, 28(20): 2112-2118. https://doi.org/10.1038/onc.2009.71

34. Tollinger, M., Crowhurst, K.A., Kay, L.E. & Forman-Kay, J.D. 2003. Site-specific contributions to the pH dependence of protein stability. *Proceedings of the National Academy of Sciences*, 100(8), 4545-4550. https://doi.org/10.1073/pnas.0736600100

35. Traven, A. & Heierhorst, J. 2005. SQ/TQ cluster domains: concentrated ATM/ATR kinase phosphorylation site regions in DNA-damage-response proteins. *Bioessays*, 27(4), 397-407. https://doi.org/10.1002/bies.20204

36. Wilkins, M.R., Gasteiger, E., Bairoch, A., Sanchez, J.C., Williams, K.L., Appel, R.D. & Hochstrasser, D. F. 1999. Protein Identification and Analysis Tools in the ExPASy Server. *Methods in Molecular Biology,* 112: 531-532. https://doi.org/10.1385/1-59259-584-7:531

37. Van Zundert, G.C.P., Rodrigues, J.P.G.L.M., Trellet, M., Schmitz, C., Kastritis, P.L., Karaca, E., Melquiond, A.S.J. & Bonvin, A.M.J.J. 2016. The HADDOCK2. 2 web server: user-friendly integrative modeling of biomolecular complexes. *Journal of molecular biology*, 428(4): 720-725. https://doi.org/10.1016/j.jmb.2015.09.014

38. Yogosawa, S. & Yoshida, K. 2018. Tumor suppressive role for kinases phosphorylating p53 in DNA damage-induced apoptosis. *Cancer science*, 109(11): 3376-3382. https://doi.org/10.1111/cas.13792

39. Zhou, H.X. & Pang, X. 2018. Electrostatic interactions in protein structure, folding, binding, and condensation. *Chemical reviews*, 118(4): 1691-1741. https://doi.org/10.1021/acs.chemrev.7b00305